# Chemical structure of vanadium-based contact formation on n-AlN

S. Pookpanratana[1], R. France[2], M. Blum[1], A. Bell[3], M. Bär[1,4], L. Weinhardt[5], Y. Zhang[1], T. Hofmann[1], O. Fuchs[5], W. Yang[6], J. D. Denlinger[6], S. Mulcahy[3], T. D. Moustakas[2], and C. Heske[1]

[1] Dept. of Chemistry, University of Nevada Las Vegas (UNLV), Las Vegas NV 89154-4003
[2] Dept. of Electrical and Computer Engineering, Boston University, Boston MA 02215
[3] Dept. of Geosciences, University of Nevada Las Vegas, Las Vegas NV 89154-4010
[4] Solar Energy Research, Helmholtz-Zentrum Berlin für Materialien und Energie GmbH, 14109 Berlin, Germany
[5] Experimentelle Physik VII, Universität Würzburg, 97074 Würzburg, Germany
[6] Advanced Light Source (ALS), Lawrence Berkeley National Laboratory, Berkeley, CA 94720

**Abstract:**

We have investigated the chemical interaction between a Au/V/Al/V layer structure and n-type AlN epilayers using soft x-ray photoemission, x-ray emission spectroscopy, and atomic force microscopy. To understand the complex processes involved in this multi-component system, we have studied the interface before and after a rapid thermal annealing step. We find the formation of a number of chemical phases at the interface, including VN, metallic vanadium, aluminum oxide, and metallic gold. An interaction mechanism for metal contact formation on the entire n-(Al,Ga)N system is proposed.

## I. Introduction

N-type $Al_xGa_{1-x}N$ alloys are of high interest due to their applications in optoelectronic devices, such as light emitting diodes [1, 2, 3, 4]. In such devices, forming Ohmic contacts is of large importance. However, this is a significant fundamental challenge for these materials. First, the electron affinity of GaN (3.3 eV) and AlN (1.9 eV) are very different [5], and thus it is difficult to find *one* contact scheme compatible for the entire $Al_xGa_{1-x}N$ ($0 \leq x \leq 1$) alloy system. Vanadium-based contacts involving rapid thermal annealing (RTA) were first used on n-$Al_{0.3}Ga_{0.7}N$, and it was found that optimal contact formation occurred at less severe conditions (*i.e.*, lower processing temperatures) compared to Ti-based contacts [6]. However, it was found that, with increasing Al content in the alloy, the optimal RTA temperature had to be increased for optimal specific contact resistivity [7]. Second, the employed contact schemes are very complex and empirically derived. Consequently, a deeper understanding of the underlying interface formation processes and insights into the character of interface species and secondary phases is lacking. Such understanding, however, is needed to further optimize the interfaces and thus performance of associated devices. While, thus, the motivation of this study is an applied one, the main goal of this work is to gain a fundamental understanding of the chemical interface processes during high-temperature annealing.

For a deeper insight into the interface properties, we have employed a unique combination of spectroscopic and microscopic tools. In particular, we have used x-ray photoelectron spectroscopy (XPS) and x-ray emission spectroscopy (XES) to study the local chemical environment at the surface and near-surface bulk in an atom-specific fashion. These

techniques have previously been used successfully to shed first light on the V-based contact formation on n-GaN [8]. XES has also been widely used to investigate the electronic structure of GaN, AlN, and their alloys [9, 10, 11]. Here, XES was used to investigate the local atomic environment of nitrogen and vanadium of Au/V/Al/V/n-AlN structures before and after RTA treatment. Since XES is a photon-in-photon-out technique, it can probe the surface-near bulk and buried interfaces within the top tens to a few hundreds of nanometers. In addition, the surface composition before and after annealing was monitored by XPS. Furthermore, we have employed atomic force microscopy (AFM) in air to study the surface morphology before and after interface formation, and wavelength-dispersive x-ray spectroscopy (WDS) to investigate the lateral distribution (in the form of maps) of atomic species at the surface.

By combining the results from these complementary experimental approaches, we are able to depict a detailed model of the interface structure. As will be shown in Section III, this structure is very complex and therefore requires the combination of such fundamental and sophisticated techniques to gain a comprehensive picture.

## II. Experiment

Si-doped AlN samples were grown by molecular beam epitaxy onto c-plane sapphire. Subsequently, metal layers were deposited by electron beam evaporation. Additional details of sample growth and preparation have been published elsewhere [7]. The Au/V/Al/V contact scheme (where Au is the topmost layer) consisted of Au(100 nm)/V(20 nm)/Al(80 nm)/V(15 nm) (all thicknesses given are nominal values). Samples were cut into two parts, one of which was RTA-treated (1000 °C for 30 seconds in $N_2$). The samples were then packed and sealed under dry nitrogen without air exposure (to minimize any external surface contamination) and shipped

from Boston University to UNLV. Samples were unloaded without air exposure in an $N_2$-purged glovebox prior to direct transfer into the ultra-high vacuum (UHV) chamber for XPS analysis. For the less surface-sensitive XES experiments, samples were briefly (< 10 minutes) exposed to air prior to transfer into the UHV chamber at the ALS. AFM experiments (Park XE70 contact mode) were conducted in air after completion of the XPS and XES experiments, and followed by WDS.. Reference materials (VN powder, metal foils) were obtained from Alfa Aesar .

XES experiments were performed at Beamline 8.0.1 at the Advanced Light Source (ALS), Lawrence Berkeley National Laboratory, in our SALSA endstation [12]. SALSA is equipped with a high-resolution, high-transmission variable line spacing soft x-ray spectrometer (further details of the instrument can be found elsewhere [13]). XPS experiments were carried out at UNLV using a Mg $K_\alpha$ radiation x-ray source and a SPECS 150MCD Phoibos electron analyzer. The energy scale of the analyzer was calibrated using XPS and Auger lines of Au, Ag, and Cu [14]. Elemental WDS and backscattered electron (BSE) mapping was run at the UNLV EMIL facility with a JEOL electron probe microanalyzer JXA-8900. The Au $M_\alpha$, V $K_\alpha$, and Al $K_\alpha$ fluorescence lines were detected simultaneously with three wavelength-dispersive spectrometers using lithium fluoride (for Au $M_\alpha$ and V $K_\alpha$) and thallium acid phthalate (TAP, for Al $K_\alpha$) analyzing crystals, and an acceleration voltage of the excitation electron beam of 20 kV at a beam current of 100 nA.

## III. Results and Discussion

In Fig. 1, N K XES spectra of an untreated and an RTA-treated sample are shown, along with n-AlN (epilayer) and VN (powder) reference spectra. The spectrum of the untreated sample

was multiplied by 8000 to account for the significant x-ray attenuation in the metallic overlayers - the attenuation length (*i.e.*, the film thickness that attenuates an x-ray beam to 1/e of its initial intensity) at 392 eV is 35 nm in Au, 323 nm in V, and 273 nm in Al [15]. This demonstrates the unique capability of XES to probe a buried system, even through a metal layer stack of a nominal thickness of 215 nm. The intensity of the N K XES spectrum after annealing is substantially increased due to morphological changes described below.

The energy of the main peak in the N K spectrum for both, the untreated and the RTA-treated sample, agrees well with that of n-AlN. In fact, at first glance, the emission of the RTA-treated sample looks nearly identical to that of n-AlN, but closer inspection reveals a broad shoulder of low intensity around 391 eV, best seen in the difference spectrum (RTA – n-AlN, magnified by 3) shown above the VN reference spectrum. This feature coincides with the main peak seen in the VN spectrum. To quantify the contributions from AlN and VN to the N XES spectrum, the spectrum of the RTA-treated sample is compared to a sum spectrum that was computed using the spectra of the n-AlN and VN references. This sum spectrum is also shown in Fig. 1 (top, red solid line), along with the measured data, the AlN and VN contributions, the residual (*i.e.*, the difference between the data and the fit), and the utilized weight factors (which were determined with a least-square fit routine to minimize the residual). The result shows that 82% of the peak area can be described with the n-AlN spectrum, and the rest (18%) with the VN spectrum. Note that we do not attempt to interpret the lineshape of the (very weak) peak of the untreated sample, since it is most likely obscured by background effects that can be neglected for all other (significantly more intense) peaks.

An additional indicator for the presence of VN in the RTA-treated sample is the observation of a 'knee' at higher energies (~396-397 eV, see amplified region above the RTA spectrum). This feature is also present in VN, but not in AlN, as can be seen from the amplified region shown above the n-AlN spectrum in Fig. 1. The feature is ascribed to valence electrons at and near the Fermi energy and their relaxation into the N 1s core hole (note that VN is considered to exhibit metallic character [16, 17, 18, 19]). Thus, we conclude that the nitrogen atoms probed in the RTA-treated sample are present as AlN and partially transformed to VN as a result of the RTA treatment.

V $L_3$ XES suggests the formation of VN in the RTA-treated sample as well. The V $L_3$ spectra of the samples are shown in Fig. 2, along with a V metal and a (modified) VN reference spectrum. For the VN reference (referred to as "VN mod."), we modified the spectrum of the as-received VN powder (Alfa Aesar) to account for the observed surface oxidation by subtracting a suitably weighted V $L_3$ spectrum of a $VO_2$ reference. The weight was chosen based on the integrated area ratio for the O K emission in the $VO_2$ and the (oxidized) VN spectra (not shown) to approximate a "pure" VN spectrum.

The untreated sample has a V $L_3$ emission energy and (broad) shape similar to that of vanadium metal (as expected). The spectrum has a very low signal-to-noise ratio, since the V emission stems from atoms below at least (nominally) 100 nm of Au (the 1/e attenuation length at 510 eV in Au is about 43 nm [15]). Upon RTA treatment, the spectrum undergoes pronounced changes, most notably a substantial increase in intensity and an additional emission feature at lower energies. To understand the origin of this feature, a sum spectrum was computed using the VN (mod.) and V metal reference spectra and suitable weight factors to describe the RTA data

(shown in Fig. 2, top portion). The weight factors were again determined with a fit, and it was found that the RTA spectrum can be best described with 76% of the area from a VN (mod.) contribution, and 24% from V metal. Thus, most of the probed V atoms exist in a VN environment, while some remain unreacted in a V metal environment. Note that we do not find any direct indication of the presence of vanadium oxide, but small amounts might nevertheless be present (since there is some uncertainty in the "purity" of the VN mod. spectrum, as discussed above).

To summarize the XES results, we find the formation of VN as a result of the RTA treatment, and also detect the presence of metallic V and of AlN in the probed volume.

In order to complement these findings with very surface-sensitive information, the surface composition before and after RTA treatment was analyzed using XPS. Fig. 3a shows the corresponding XPS survey spectra. As expected, the untreated sample surface is dominated by Au lines (*i.e.*, from the topmost layer in the metal layer structure). Upon RTA treatment, the Au signals are significantly reduced, and previously buried elements (Al, V, and N) are now detected on the surface. This finding suggests significant interdiffusion processes and/or morphological changes as a result of the RTA-treatment, which will be further discussed in the following. We also note that, despite the efforts to minimize surface contamination (as described in the experimental section), both samples exhibit signals from C and O species on the surface. While the carbon signal is reduced after annealing, the oxygen signal is significantly enhanced, as evidenced by the increase of both the O 1s photoemission line as well as the O KLL Auger emission. Apparently, an oxide species has formed on the surface during the annealing step. In

order to shed light on the chemical nature of the surface oxide, detail spectra were recorded for all metal lines observed in the survey spectra.

In Fig. 3b, the Al 2p region is shown for the annealed sample and an oxidized Al metal foil reference (the Al foil was scratched in a $N_2$ filled glove box prior to transfer into UHV to also expose some metallic Al atoms at the surface). Note that the Al 2p feature was not detected in the untreated sample because of attenuation in the Au top layer.

Due to the Mg $K_{\alpha_3}$ and $K_{\alpha_4}$ excitation satellites of the (non-monochromatized) x-ray source, the as-measured spectrum of the annealed sample has satellite contributions from the Au 4f lines in the Al 2p spectral window. To subtract these satellite lines, a sputter-cleaned Au reference foil was measured in the same energy window, and the spectrum was subtracted from the spectrum of the RTA-treated sample (after normalizing both spectra to the Au $4f_{7/2}$ main peak height). The result of this subtraction is shown in Fig. 3b.

The oxidized Al metal reference foil has two components contributing to the Al 2p region - the feature at lower binding energies is due to metallic Al, while the one at higher binding energies is a native aluminum oxide, most likely $Al_2O_3$ (as it is thermodynamically most stable). The energetic positions of the two features are in agreement with the chemical shift reported between metallic Al and $Al_2O_3$ (+2.7 – 2.8 eV [20, 21, 22]). Note that the spin-orbit splitting of the $2p_{1/2}$ and $2p_{3/2}$ (0.4 eV [23]) cannot be resolved in our measurements, since it is small compared to the experimental linewidth (dominated by the width of the excitation source) and likely further obscured by the presence of Al in (slightly) differing oxidation states.

As is apparent from the excellent agreement between the binding energy of the Al 2p peak of the annealed sample and the aluminum oxide peak of the Al reference foil, we find that

the Al atoms at the surface are not metallic, but exclusively in oxide form. This explains the significant increase in O 1s intensity; however, we note that, additionally, other oxides may exist. In particular, we cannot completely rule out the presence of some vanadium oxide – the peak position and lineshape analysis of the V 2p photoemission and V LMM Auger lines is inconclusive, most likely due to the presence of both a VN and a metallic V species (in addition to a potential vanadium oxide).

To summarize the XPS findings, we note a significant change in surface composition after annealing, corroborating the XES-derived interpretation of significant interdiffusion processes and/or morphological changes as a result of the RTA-treatment. We find a substantial reduction in the Au surface intensity, an increase of the V, Al, N, and O signals, and the clear presence of an aluminum oxide on the surface.

To supplement the compositional and chemical information derived from the spectroscopic data, we have collected contact-mode AFM images (Figs. 4a and b), a BSE map (Fig. 4c), and WDS elemental maps of Al, Au, V (Figs. 4d-f) to derive the surface morphology and lateral elemental distribution. The AFM images of the untreated sample (Fig. 4a) exhibit a very flat surface (maximum elevation about 10 nm), covered with closely packed grains (with typical diameter of 100 nm), as expected for a thick metal overlayer and in agreement with the XPS information. In contrast, the surface of the annealed sample in Fig. 4b is rough (maximum elevation about 1.4 μm), with an inhomogeneous lateral distribution of large (approximately 7 μm in diameter) clusters and small (approximately 1-2 μm in diameter) clusters in-between. In the vertical dimension, the large clusters are about 1.4 μm higher than the lowest (darkest) regions. For the small clusters, this height is about 270 nm from the lowest regions.

The BSE map in Fig. 4c shows a similar structure, albeit at a different location on the sample. At the ”BSE location”, the WDS maps show that the large clusters are mostly composed of Au (Fig. 4e), with some contribution of V (Fig. 4f; this is most easily seen for the three pronounced clusters in the bottom left corner or the three clusters at the bottom right edge of the maps). We note that the distribution of V is “spotty” – apparently, islands or subclusters containing V are formed. As is evident from the Al and Au maps (Fig. 4d and 4e), their distribution is anti-correlated – for example, the three clusters with high Au and (spotty) V intensity correspond to low intensities in the Al map. Note that the 1/e attenuation length of the Al $K_\alpha$ fluorescence used for this map is between 162 nm (in pure Au) and 480 nm (in pure V) [15]. Thus, this finding suggests the absence of Al in the large clusters, while it does not rule out the presence of Al atoms *underneath* the big clusters, *i.e.*, in the n-AlN substrate.

In combining the results from the various elemental, chemical, and topographic probes, we are now able to paint (propose) a comprehensive picture of the interface structure between the metal overlayers and the n-type AlN film after annealing. From the AFM images, we find that the contact layers transform from a nanocrystalline closed layer to a surface with two types of clusters (“large” and “small”). From the WDS elemental mapping, we find that the large clusters are mostly composed of Au with some inhomogeneous V enclosures or islands. From the XES analysis, we know that these V regions contain vanadium in both, a metallic and a VN-like environment. In contrast to the large clusters, the small clusters show a strong Al signal and minimal Au and V intensity. From the XPS analysis, we know that these Al atoms (at least those at the surface) are exclusively in an aluminum oxide environment. The (laterally integrated) XPS intensity analysis shows that annealing leads to morphological changes that allow previously

buried elements (N, Al, and V) to be detected at the surface, and, as mentioned, the AFM images and WDS maps can then be used to correlate this information with laterally-resolved insights, as described above.

The findings are summarized in the schematic structure shown in Fig. 5. During the annealing process, the atoms of the metallic top layers become very mobile and diffuse to form a very different surface morphology. Au and V atoms migrate to form large clusters (with the V being present in both metallic and VN form), while Al atoms migrate to form small clusters, presumably forming an aluminum oxide, and leading to an increased number of grain boundaries. The effective overall thickness of the "cover layer" is thus reduced, so that, *e.g.*, the AlN substrate becomes "visible" in XES. As mentioned, the XES analysis confirms the formation of VN as a result of the RTA treatment. For reasons discussed below, we speculate that the nitrogen source for this VN formation is likely the AlN layer, and that thus the VN is located at the interface between the large clusters and the AlN substrate. Also, note that the WDS maps show an inhomogeneous lateral V distribution within the large clusters (not shown in Fig. 5).

As mentioned, we speculate that the nitrogen source for the VN formation is the AlN substrate (and not the ambient $N_2$ molecules during the RTA step). For n-GaN, we could previously show the presence of metallic Ga at the (Au, V, Al)/GaN interface, suggesting that the nitrogen source was indeed the GaN substrate [8]. In the present case, a similar experimental argument cannot be applied, since the Al signal is vastly dominated by the Al atoms in the AlN substrate, and because Al is additionally present in the (initial) contact scheme. France *et al*. found that for optimal contact resistivity in the (Al,Ga)N alloy system, the required RTA processing temperature increases with increasing Al content – varying from 650°C (pure n-GaN)

to 1000°C (pure n-AlN) [7]. It was hypothesized that the RTA temperature was related to the bond strength ($E_b$) of Ga-N and Al-N [7]. Indeed, Talwar *et al*. report that $E_{b,Al-N} > E_{b,Ga-N}$ [24]. If we assumed that ambient $N_2$ molecules serve as the nitrogen source for VN formation, then the processing temperature should be independent of alloy composition since the V-N interaction is independent of the underlying substrate material (GaN or AlN). Since the optimal RTA processing temperature is reported to be dependent on the (Al,Ga)N composition, it is thus very unlikely that the ambient $N_2$ plays a significant role as a nitrogen source. In contrast, this analysis suggests the n-(Al,Ga)N alloy as the nitrogen source for VN formation, as in the case of n-GaN [8].

These findings shed light on the fundamental interactions between metal contact layers and the n-(Al,Ga)N alloy system during annealing. The N K XES spectra of n-GaN show the nitrogen atoms in a dominant VN chemical environment [8], while for n-AlN, the N is dominant in an AlN environment with some VN contributions (note that the metal contact schemes in the two experiments were identical). For the n-GaN, the vanadium was mostly found in a metallic state, with some VN also being found [8], while in the case for n-AlN the converse is true. Furthermore, we find very different morphologies in the two cases – the n-GaN-based system forms a vein-like network after RTA treatment [8], while in the n-AlN case, we observe large and small clusters. This indicates that contact formation on the (Al,Ga)N alloy system occurs differently for varying Al content. A possible explanation could be based on thermodynamic stability. The standard heat of formation ($\Delta H_{298K}$) for GaN, VN, and AlN is -109.7 kJ/mol, -217.3 kJ/mol, and -318.6 kJ/mol, respectively [25]. Since the heat of formation of VN is more negative

than that of GaN, it is energetically more favorable to utilize a limited number of N atoms to form VN rather than GaN.

In contrast, the heat of formation of AlN is more negative than that of VN, and thus the formation of AlN is favored over that of VN in a situation of limited nitrogen abundance. Thus, these simple thermodynamic considerations can explain the dominant contribution of VN to the N K XES spectrum in the annealed n-GaN system, while for the RTA-treated n-AlN system, the AlN contribution still dominates the nitrogen spectrum over VN. Nevertheless, some VN is formed in the annealing process of AlN as well. In order to supply sufficient energy for this (nominally) endothermic process, thermal energy is required, and thus optimal (Ohmic) metal contacts on n-AlN presumably require higher RTA temperatures than in the n-GaN case.

## IV. Summary

We have investigated the interaction between Au/V/Al/V metal contact layers and n-AlN upon annealing using a combination of spectroscopic and microscopy techniques (XES, XPS, WDS, BSE, and AFM). We have confirmed the previously speculated formation of VN as a result of the annealing step, and find significant morphological changes that lead to the formation of large and small clusters with significantly different elemental and chemical composition. Large clusters are composed of Au and an inhomogeneous distribution of V atoms in metallic and VN environments. Small clusters are composed of aluminum oxide. We have provided arguments that the nitrogen source for the VN formation is the AlN substrate and not the ambient nitrogen molecules during annealing. Finally, we have discussed the thermodynamical considerations

governing the formation of GaN, VN, and AlN, and thus shed light on the metal contact interaction mechanism for the entire n-(Al,Ga)N alloy system.

**Acknowledgements**

We gratefully acknowledge support from the U.S. Department of Energy (DOE) under contract DE-FG36-05GO85032 and the Nevada System of Higher Education under SFFA No. NSHE 07-101 and 08-03. The Advanced Light Source is supported by the Director, Office of Science, Office of Basic Energy Sciences, of the U.S. Department of Energy under Contract No. DE-AC02-05CH11231.

## References


[1] S. Nakamura, T. Mukai, and M. Senoh, *Appl. Phys. Lett*. **64**, 1687 (1994).

[2] F. A. Ponce and D. P. Bour, *Nature* **386**, 351 (1997).

[3] S. Nakamura, M. Senoh, S. Nagahama, N. Iwasa, T. Yamada, T. Matsushita, H. Kiyoku, Y. Sugimoto, T. Kozaki, H. Umemoto, M. Sano, and K. Chocho, *Appl. Phys. Lett.* **72**, 2014 (1998).

[4] E. Monroy, M. Hamilton, D. Walker, P. Kung, F. J. Sanchez, and M. Razeghi, *Appl. Phys. Lett*. **74**, 1171 (1999).

[5] C. I. Wu and A. Kahn, *Applied Surface Science* **162-163**, 250 (2000).

[6] K. O. Schweitz, P. K. Wang, S. E. Mohney, and D. Gotthold, *Appl. Phys. Lett.* **80**, 1954 (2002).

[7] R. France, T. Xu, P. Chen, R. Chandrasekaran, and T. D. Moustakas, *Appl. Phys. Lett.* **90**, 062115 (2007).

[8] S. Pookpanratana, R. France, M. Bär, L. Weinhardt, M. Blum, O. Fuchs, W. Yang, J. D. Denlinger, T. D. Moustakas, and C. Heske, *Appl. Phys. Lett.* **93**, 172106 (2008).

[9] C. B. Stagarescu, L.-C. Duda, K. E. Smith, J. H. Guo, J. Nordgren, R. Singh, and T. D. Moustakas, *Phys. Rev. B* **54**, 335 (1996).

[10] L. C. Duda, C. B. Stagarescu, J. Downes, K. E. Smith, D. Korakakis, T. D. Moustakas, J. Guo, and J. Nordgren, *Phys. Rev. B* **58**, 1928 (1998).

[11] M. Magnuson, M. Mattesini, C. Höglund, J. Birch, and L. Hultman, *Phys. Rev. B* **80**, 155105 (2009).

[12] M. Blum, L. Weinhardt, O. Fuchs, M. Bär, Y. Zhang, M. Weigand, S. Krause, S. Pookpanratana, T. Hofmann, W. Yang, J. D. Denlinger, E. Umbach, and C. Heske, *Rev. Sci. Instrum*. **80**, 123102 (2009).

[13] O. Fuchs, L. Weinhardt, M. Blum, M. Weigand, E. Umbach, M. Bär, C. Heske, J. Denlinger, Y.-D. Chuang, W. McKinney, Z. Hussain, E. Gullikson, M. Jones, P. Batson, B. Nelles, and R. Follath, *Rev. Sci. Instrum.* **80**, 063103 (2009).

[14] M. T. Anthony and M. P. Seah, *Surf. and Interface Analysis* **6**, 107 (1984).

[15] B. L. Henke, E. M. Gullikson, and J. C. Davis, *Atomic Data Tables* **54**, 181-342 (1993). http://henke.lbl.gov/optical_constants/atten2.html

[16] D. W. Fischer, *J. Appl. Phys*. **40**, 4151 (1969).

[17] A. Callenaś, L. I. Johansson, A. N. Christensen, K. Schwarz, and P. Blaha, *Phys. Rev. B* **32**, 575 (1985).

[18] R. Fix, R. G. Gordon, and D. M. Hoffman, *Chem. Mater.* **5**, 614 (1993).

[19] R. Sanjinés, P. Hones, and F. Lévy, *Thin Solid Films* **332**, 225 (1998).

[20] D. Briggs and M. P. Seah, *Practical Surface Analysis by Auger and X-ray Photoelectron Spectroscopy*, (John Wiley & Sons, Chichester, 1983), p. 487.

[21] A. Barrie, *Chem. Phys. Lett*. **19**, 109 (1973)

[22] R. Z. Bachrach, S. A. Flodström, R. S. Bauer, S. B. M. Haström, and D. J. Chadi, *J. Vac, Sci. Technol.* **15**, 488 (1978).

[23] A. Thompson, D. Vaughan, D. Attwood, E. Gullikson, M. Howells, K.-J. Kim, J. Kirz, J. Kortright, I. Lindau, Y. Liu, P. Pianetta, A. Robinson, J. Scofield, J. Underwood, G. Williams,

and H. Winick, *X-ray Data Booklet*, (Lawrence Berkeley National Lab, Berkeley, 2009) p. 1-2. http://xdb.lbl.gov/

[24] D. N. Talwar, D. Sofranko, C. Mooney, and S. Tallo, *Materials Science and Engineering* **B90**, 269 (2002).

[25] *Smithell's Metal Reference Book*, (Buttersworth, London, 1985), p. 8-23 – 8-24.

**Figure Captions**

Fig. 1. N K XES spectra of the untreated (data points and Fourier-smoothed curve) and RTA-treated (data only) sample, together with n-AlN andVN reference spectra. Above the VN spectrum, the difference (magnified) between the RTA-treated and the n-AlN spectrum (normalized to area) is shown. For the n-AlN and the RTA spectrum, an enlarged (× 6) view of the uppermost valence band region is also shown. The top portion of the graph shows a fit (solid red line) of the RTA-treated sample data (dots) using a sum of the n-AlN (blue, 82% area fraction) and VN (green, 18% area fraction) spectra. The residual of the fit, magnified by a factor of 5, is also shown.

Fig. 2. V $L_3$ XES spectra of the untreated (data points and Fourier-smoothed curve) and RTA-treated (data only) sample, together with V metal and VN reference spectra. The VN spectrum is designated as modified ("mod."), because a vanadium oxide contribution was removed (for details see text). The top portion of the graph shows a fit (solid red line) of the RTA-treated sample data (dots) using a sum of the V metal (magenta, 24% area fraction) and the modified VN (green, 76% area fraction) spectra. The residual of the fit is also shown, multiplied by 2.

Fig. 3. (a) XPS survey spectra of the untreated and RTA-treated sample, and (b) detail spectra of the Al 2p region of the RTA-treated sample and an oxidized Al metal foil.

Fig. 4. 40 x 40 $\mu m^2$ images of the untreated sample, acquired by (a) AFM (contact mode in air; inset shows a 1 x 1 $\mu m^2$ image), images of the annealed sample acquired by (b) AFM, (c) using back-scattered electrons (BSE), and (d)-(f) WDS. Images (c) – (f) were collected from the same location on the sample, while (b) was taken at a different location. The maximal AFM z-scale (elevation) between the dark (low) and white (high) areas is about 10 nm for (a) and about 1.4 μm for (b). The WDS maps show the elemental distribution (fluorescence intensity) of (d) Al, (e) Au, and (f) V. The intensity scale follows the colors of the electromagnetic spectrum (black and blue: low; red and white: high).

Fig. 5. Schematic of metal/n-AlN contact structure before and after rapid thermal annealing.

**Figures**

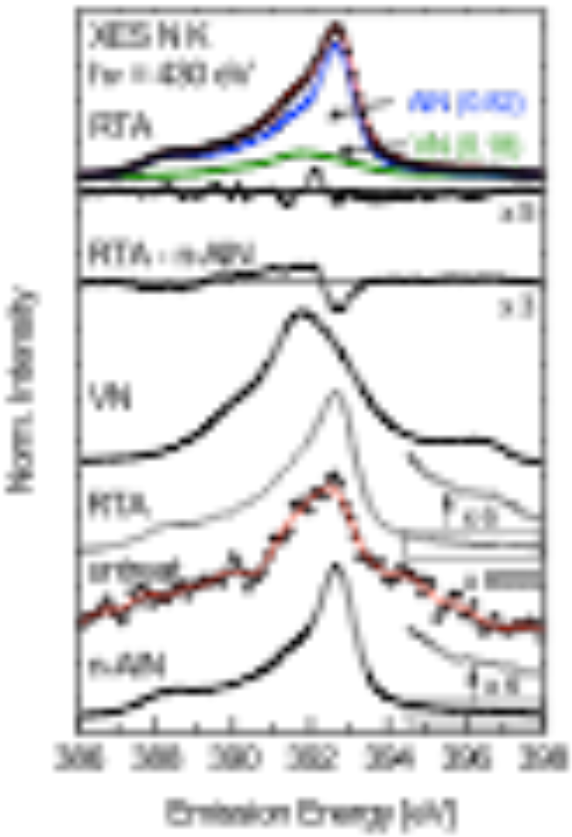


Fig. 1, Pookpanratar

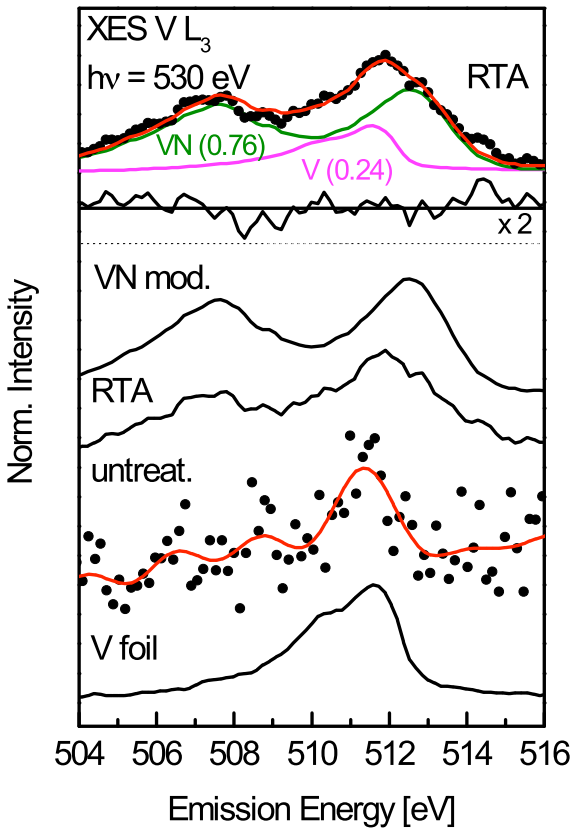


Fig. 2, Pookpanratana et al.

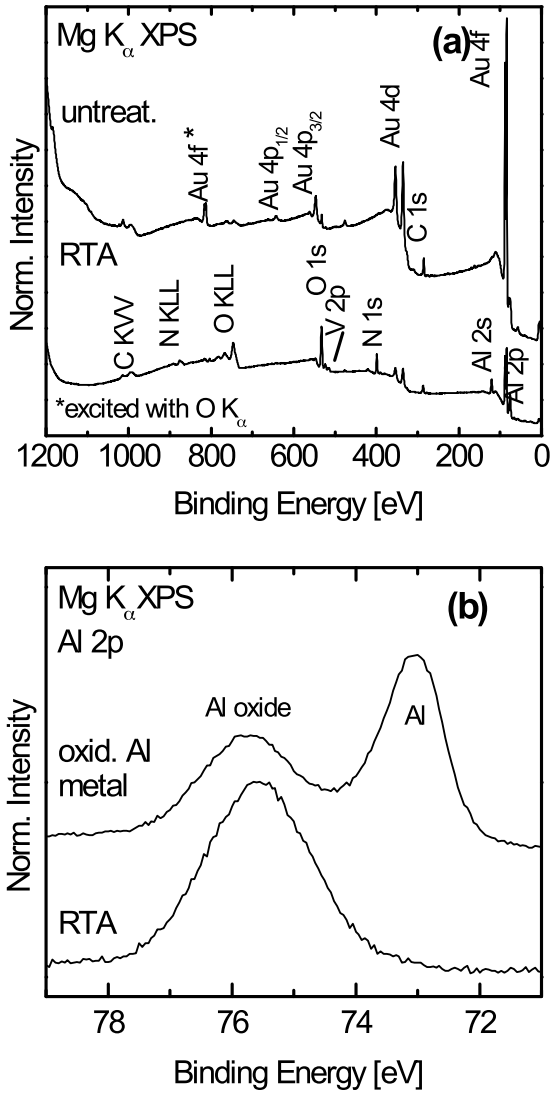


Fig. 3, Pookpanratana et al.

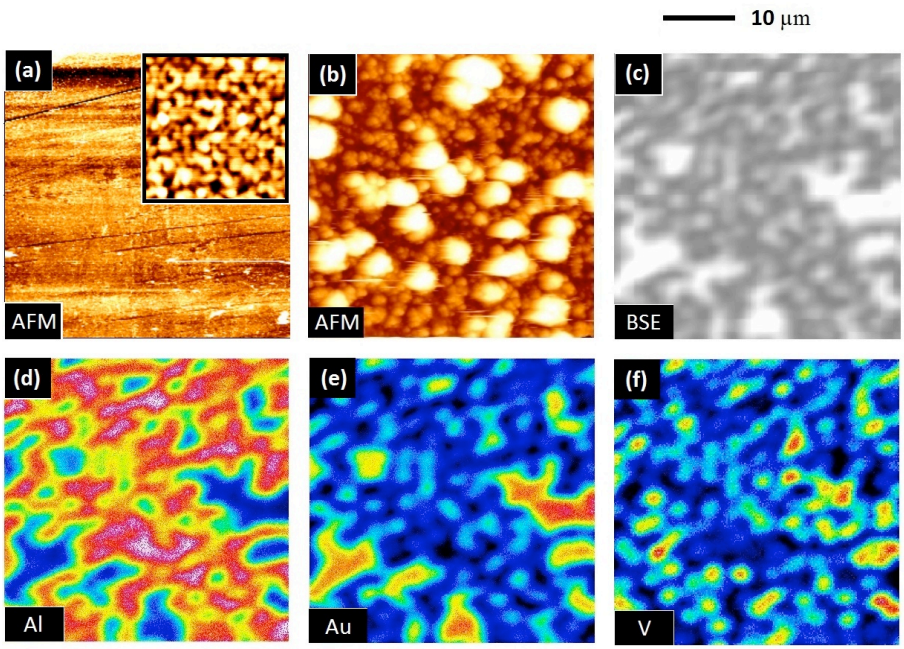


Fig. 4, Pookpanratana et al.

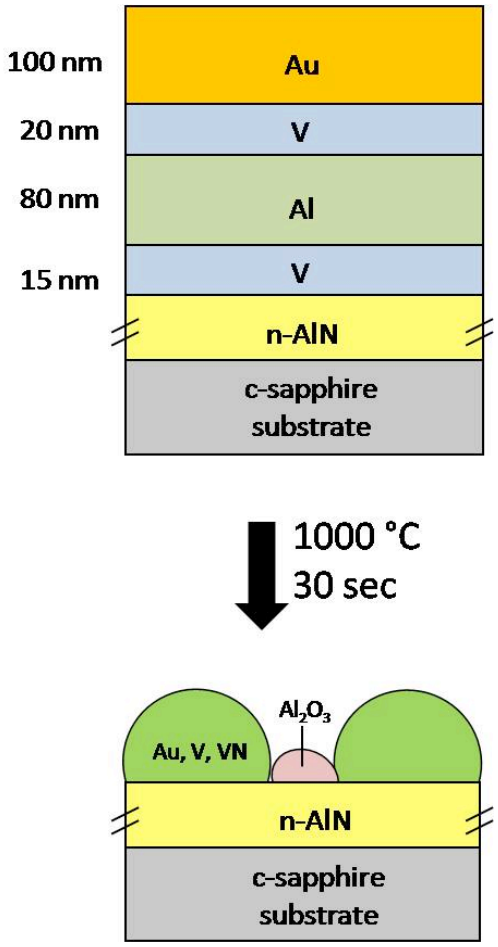


Fig. 5. Pookpanratana et al.